# Is helium the key parameter in the extended color spread of the first generation stars in M3?

M. Tailo[1],[*] F. D'Antona[2], V. Caloi,[3] A. P. Milone[1], A. F. Marino[1,4], E. Lagioia[1], G. Cordoni[1]

[1] *Dipartimento di Fisica e Astronomia "Galileo Galilei", Univ. di Padova, Vicolo dell'Osservatorio 3, Padova, IT-35122*
[2] *INAF – Osservatorio Astronomico di Roma, via di Frascati 33, Monte Porzio Catone, IT-00078*
[3] *INAF – IASF Roma, Via Fosso del Cavaliere, Roma, Italy, IT-00133*
[4] *Centro di Ateneo di Studi e Attivita' Spaziali "Giuseppe Colombo" - CISAS, Via Venezia 15, Padova, IT-35131*

**ABSTRACT**

The study of the "chromosome maps" of Galactic Globular Clusters has shown that the stars identified as 'first generation' often define an extended sequence in the $m_{F275W} - m_{F814W}$ colour, whose straightforward interpretation, by comparison with synthetic spectra, is that they are inhomogeneous in helium content. The cluster M 3 (NGC 5272) is one of the most prominent example of this phenomenon, since its first generation is distributed on an extended colour range, formally corresponding to a large helium enhancement ($\sim 0.1$). It is necessary to ask whether the bulk of photometric observations available for this cluster supports or falsifies this interpretation. For this purpose, we examine the horizontal branch morphology, the period and magnitude distributions of the RR Lyrae variables, and the main sequence colour distribution. Simulating the first generation stars with such internal variation of helium content we can not meet all the observational constraints at the same time, concluding that the origin of the first generation colour spread is still without a straightforward explanation.

**Key words:** (stars:) Hertzsprung-Russell and colour-magnitude diagrams, stars: horizontal branch, stars: variables: RR Lyrae, (Galaxy:) globular clusters: general, (Galaxy:) globular clusters: individual:NGC5272,

## 1 INTRODUCTION

The rich mine of the *Hubble Space Telescope (HST)* UV Legacy Survey of Globular clusters data (GC, Piotto et al. 2015) allowed to build a "chromosome map" (ChM) for each cluster, by plotting for each star specific combination of UV and optical–near infrared HST bands (a detailed description of the procedure used can be found in Milone et al. 2017). These maps constitute a powerful spectro-photometric tool to distinguish different stellar populations in GCs, but they have unveiled patterns that lack a satisfying explanation in the context of GCs evolution. A prominent example is the fact that Milone et al. (2015, 2017) first, then Lardo et al. (2018) and Milone et al. (2018) found that the first generation of star (1G), as defined by the ChMs, in several cases does not look compatible with a homogeneous population.

In fact, the 1G stars show a dispersion in the $m_{F275W} - m_{F814W}$ colour that can be associated to variations of both

chemical and physical properties, due to the high sensibility of the special combination of filters employed. This puzzling result, first found during the analysis of the GC NGC2808 (Milone et al. 2015; D'Antona et al. 2016), and then confirmed for many other clusters by Milone et al. (2017, 2018), leaves us with the doubt that the picture of what could have been the evolutionary process that led to the formation of a GC was even more complex and confusing than we might have envisioned until now.

While the second generation (2G) in the ChMs can be interpreted as the result of CNO burning (Milone et al. 2017), the 1G stars distribution should have a different origin. Milone et al. (2015) and Lardo et al. (2018) tentatively attributed it to pure helium differences among the 1G stars. Although following similar comparison with synthetic spectra, finding maximum values of helium enhancements ranging from $\sim 0.00$ to $\sim 0.10$, Milone et al. (2018) were very doubtful on the feasibility of this explanation, based on simple theoretical grounds. Nevertheless, recently Cabrera-Ziri et al. (2019) have obtained the abundances of C, N, O, Na,
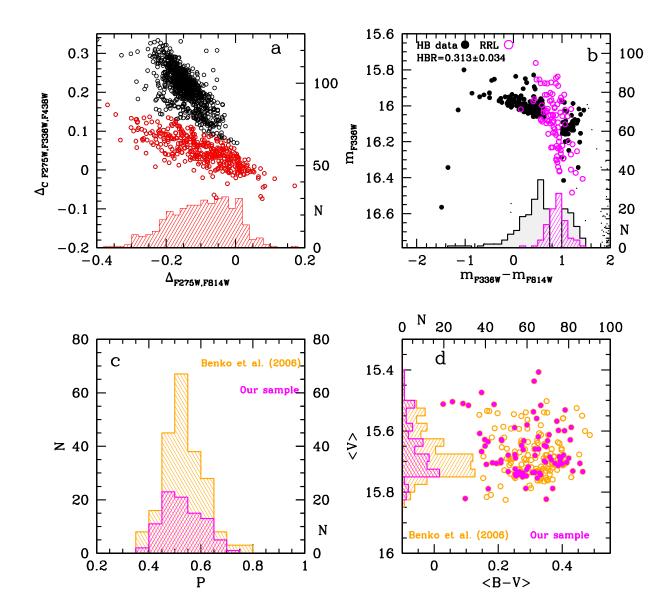
[*] E-mail: marco.tailo@unipd.it; mrctailo@gmail.com

**Figure 1.** *Panel a:* The ChM of M3 with highlighted the 1G (red) and its colour distribution. *Panel b:* The HB subsample in the *HST* data. We identify the RRL variable stars and represent them as magenta, open circles while other HB stars are plot as black, filled ones. The two histograms describe the distribution of the HB stars (black) and of the variable stars (magenta). See text for more details (§ 2.1) *Panel c:* The period distribution of the RRL variables from the global catalogue (Benkő et al. 2006, orange histogram) and of the ones in the *HST* sample (magenta histogram). The peak at P ∼ 0.53 is still present, but is not as sharp as the one in the general distribution. *Panel d:* The colour magnitude diagram, built from the mean magnitudes, of the RRL variables in the global catalogue (Benkő et al. 2006, orange). We highlighted the RRL of the *HST* sample (magenta).

Mg and Al of stars all along the extended 1G of NGC 2808, and found that they are all homogeneous in these elements, reinforcing the points made by Milone et al. (2015) using multiband photometry; this recent work then gives strenght to the proposal that the color extension of the 1G is due to pure helium enhancement. Furthermore, Marino et al. (2019), performing a combined examination of the ChM and the spectroscopic data of a large number of GCs, found the same kind of homogeneity in multiple cluster. Their inter-

pretation, on the other hand, is twofold and in addition to helium enhancement they also attribute the extended 1G sequence to iron variations. Therefore, in the absence of direct helium determination, it is important to find signatures of such a postulated helium variation by examining its influence on the location and properties of other stars in the color magnitude diagram

The cluster NGC 5272 (M 3) is a perfect example of an extended 1G (see its ChM in Milone et al. 2017, 2018). We

examine its color magnitude diagram in order to investigate whether the interpretation of the 1G extension as a result of a pure helium variation is consistent with the available observations for this GC and, most importantly, its horizontal branch (HB) and variable stars.

The stars' distribution along the HB has indeed been examined at length in the literature (e.g. Catelan 2004; Castellani et al. 2005; Caloi & D'Antona 2008; Denissenkov et al. 2017). Almost unique among the galactic GCs, M 3 has a large (>200) population of RR Lyrae variables (RRL, Corwin & Carney 2001; Benkő et al. 2006). The high sensitivity of the period distribution of these variables to any variations of the stellar parameters makes them a great probing tool for this kind of investigation.

We will achieve our goal comparing state of the art stellar population models with the most recent observations available. In doing so we will also produce a new and updated description of the HB in M3.

The present work can be divided into two main parts. In § 2 we present a summary of the observations we exploit and a description of the stellar evolution models we employ. In § 3, § 4 and 5 we present and discuss the results of our simulations. § 6 will host our conclusions and general remarks.

## 2 DATASET AND MODELS

We exploit photometry from the recent HST UV photometric survey (Piotto et al. 2015) and from the ACS survey of Galactic GCs (Anderson et al. 2008). Moreover, we used the ChM derived by Milone et al. (2017). We also employ the RRL variables database by Benkő et al. (2006). We refer to these works for the details of the data acquisition and reduction process, and the procedure used to derive the ChM of this cluster.

### 2.1 Summary of the observations

Analysing the photometric data, the ChM and its related features, Milone et al. (2018) have been able to estimate the average and the maximum value of helium enhancement between the 1G and the 2G stars ($\Delta Y_{2G,1G}$). They found $\Delta Y_{2G,1G} = 0.016 \pm 0.005$ and $\Delta Y_{2G,1G}^{max} = 0.041 \pm 0.009$ (see Table 4 in Milone et al. 2018). These values will be our first observational constraints when updating the description of the HB of this cluster.

Fig. 1a plots the ChM of M 3 from Milone et al. (2017, Figure 5), where the 1G and the 2G stars are shown as red and black dots, respectively. Figure 8 in Milone et al. (2018) shows that each element plays a distinct role in affecting the position on the ChMs. The 2G can be described as a CNO sequence, as confirmed by the spectroscopy of stars at different locations on the ChM. The prominent extension in $\Delta_{F275W,F814W}$ of the 1G of M 3 can be described by a helium enhancement sequence (Milone et al. 2015; Lardo et al. 2018; Milone et al. 2018), and would correspond to a maximum star-to-star difference in the 1G helium mass fraction $\Delta Y_{1G}^{max} \sim 0.10$ (Milone et al. 2018).

Figure 1b shows the $m_{F336W}$ versus $m_{F336W} - m_{F814W}$ colour magnitude diagram of the HB sample from the *HST* photometric catalogue. The magenta dots highlight the RRL

variables. M3 has an extended HB, stars populate both the red and the blue side of the instability strip. In the *HST* sample we count a total of $290 \pm 17.0$ HB stars divided in $54 \pm 7.4$ red HB stars, $144 \pm 12.0$ blue HB stars and $92 \pm 9.6$ RRL variables[1]. The black shaded histogram shows the colour distribution of the non variable stars. The HB ratio[2] in the *HST* sample is HBR $\sim 0.313 \pm 0.034$, significantly larger than the ratio obtained from ground based observations covering also the external parts of the cluster (HBR $\sim 0.08$, Buonanno et al. 1994; Ferraro et al. 1997; Catelan et al. 2001). This difference corroborates the evidence that blue-HB stars are more-centrally concentrated than the red HB (Catelan et al. 2001; Lee 2019). This feature is expected if the blue HB is populated by 2G stars, born more concentrated in the cluster core, as envisioned by cooling–flow formation models (e.g. D'Ercole et al. 2008) for clusters having a long relaxations time, where the stars are not fully spatially mixed (Vesperini et al. 2013). In this work we focus our investigation on the colour distribution of the non variable HB stars and the value of HBR of the *HST* sample because, in these data, the RRL variables are observed at random phases. If we want to use them to further constrain the properties of the HB stellar populations we then need to use other databases.

As already shown in Corwin & Carney (2001) and Benkő et al. (2006) both the period distribution and the average magnitude distribution of the RRLs have distinctive features. The period distribution of the 215 RRL in the Benkő et al. (2006) sample is plotted in Fig 1c (orange histogram), showing a prominent peak at P $\sim 0.53$ d. We identified the variables in common between our *HST* sample and the Benkő et al. (2006) sample, and plot their period distribution (magenta histogram). The peak at P $\sim 0.53$ d is still present, although less sharp than in the whole sample. Doing a Kolmogorov - Smirnov (KS) test we obtain a value of p $\sim 0.88$, signalling that the two distributions are indeed compatible.

We show in Fig. 1d the <V> magnitude versus <B–V> colour distribution of the whole RRL sample (orange) and of the *HST* sample. In both cases, the thickness of the instability strip is $\sim 0.20$ magnitudes (Corwin & Carney 2001; Benkő et al. 2006), and the dimmer part of the magnitude range (V>15.6) is most ($\sim 80\%$) populated. This feature was used to obtain insights on the helium content (e.g as in Caloi & D'Antona 2008; Denissenkov et al. 2017) with the results that most RRLs have been assigned to the 1G. In this case the KS test gives us a value of p $\sim 0.56$ signalling that also the two magnitude distributions are compatible

The period and mean magnitude distributions of the RRL variable stars are sensitive to any variations of the stellar parameters —in particular to possible enhancements in helium mass fraction; thus both will be an invaluable tool when we will consider the possibility that the 1G holds a large internal helium spread.

---

[1] To each of these number we associate the error estimated from the Poisson distribution.

[2] This ratio is defined as HBR=(B-R)/(B+V+R) where B,R and V are the number of blue, red and variable stars respectively.

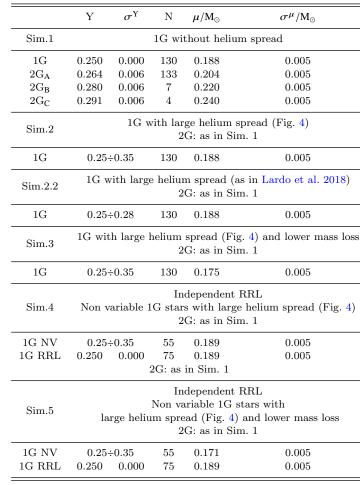| | Y | $\sigma^{Y}$ | N | $\mu/M_{\odot}$ | $\sigma^{\mu}/M_{\odot}$ |
|---|---|---|---|---|---|
| Sim.1 | | | 1G without helium spread | | |
| 1G | 0.250 | 0.000 | 130 | 0.188 | 0.005 |
| $2G_A$ | 0.264 | 0.006 | 133 | 0.204 | 0.005 |
| $2G_B$ | 0.280 | 0.006 | 7 | 0.220 | 0.005 |
| $2G_C$ | 0.291 | 0.006 | 4 | 0.240 | 0.005 |
| Sim.2 | | | 1G with large helium spread (Fig. 4) | | |
| | | | 2G: as in Sim. 1 | | |
| 1G | 0.25÷0.35 | | 130 | 0.188 | 0.005 |
| Sim.2.2 | | | 1G with large helium spread (as in Lardo et al. 2018) | | |
| | | | 2G: as in Sim. 1 | | |
| 1G | 0.25÷0.28 | | 130 | 0.188 | 0.005 |
| Sim.3 | | | 1G with large helium spread (Fig. 4) and lower mass loss | | |
| | | | 2G: as in Sim. 1 | | |
| 1G | 0.25÷0.35 | | 130 | 0.175 | 0.005 |
| Sim.4 | | | Independent RRL | | |
| | | | Non variable 1G stars with large helium spread (Fig. 4) | | |
| | | | 2G: as in Sim. 1 | | |
| 1G NV | 0.25÷0.35 | | 55 | 0.189 | 0.005 |
| 1G RRL | 0.250 | 0.000 | 75 | 0.189 | 0.005 |
| | | | 2G: as in Sim. 1 | | |
| Sim.5 | | | Independent RRL | | |
| | | | Non variable 1G stars with large helium spread (Fig. 4) and lower mass loss | | |
| | | | 2G: as in Sim. 1 | | |
| 1G NV | 0.25÷0.35 | | 55 | 0.171 | 0.005 |
| 1G RRL | 0.250 | 0.000 | 75 | 0.189 | 0.005 |

**Table 1.** The input parameters used to obtain the simulations shown in this work. Columns are: the value of helium mass fraction and its spread (Y and $\sigma^{Y}$), the number of stars in each group and the value of mass loss with its spread ($\mu$ and $\sigma^{\mu}$). A tag on the leftmost column identifies if the group of stars belongs to the 1G or the 2G and if it used for the RRL or for the red non variable stars (NV). For Sim. 2 to 5, the helium mass fraction distribution of the 1G stars is described in § 4

## 2.2 Models and simulations

The models for this work were developed in Tailo et al. (2015, 2016, 2017). While we refer to Tailo et al. (2016) for the detailed description, we remind the reader the inputs necessary to better understand the present work. The stellar evolutionary tracks have been calculated with the stellar evolution code ATON2.0 (Ventura et al. 1998; Mazzitelli et al. 1999), including the most recent updates for the physical inputs. The HB tracks and population synthesis models have been obtained following the recipes of D'Antona et al. (2002, 2005) and Caloi & D'Antona (2008).

Briefly, we fix the mass of the each star ($M^{HB}$) as follows: $M^{HB} = M_{Tip}(Z, Y, A) − \Delta M(\mu, \sigma^{\mu})$. Here $M_{Tip}$ is the mass at the red giant branch (RGB) tip, function of age (A), metallicity (Z) and helium (Y); $\Delta M$ is a Gaussian describing the mass lost by the star during the RGB phase, $\mu$ and $\sigma^{\mu}$ its central value and the standard deviation. The values of $M_{Tip}$ are obtained from the isochrone database from Tailo et al.
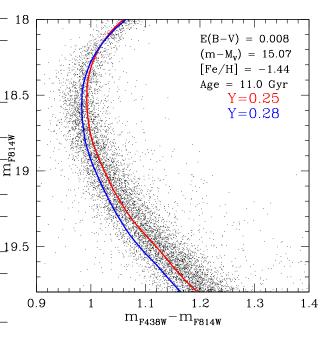


**Figure 2.** Isochrone fitting in the $m_{F814W}$ vs ($m_{F438W} − m_{F814W}$) CMD of MS stars in M3. We reported our best-fit value of E(B-V), $M_V$ and age.

(2016). When we simulate a HB stellar population with helium mass fraction spread we assume that the helium content is described by a Gaussian distribution, where Y and $\sigma^{Y}$ are the central value and the standard deviation, respectively. When calculating the properties of those stars that cross the instability strip and become RRL variables we use the prescription of Marconi et al. (2015). In simulating the mean <V> and <B> magnitude and colours of the RRL variables, we introduce the errors estimated in Benkő et al. (2006).

We select the set of models having Z=0.001 and [$\alpha$/Fe] = 0.4, corresponding to [Fe/H] ∼ −1.44 for $Z_{\odot}$ = 0.014 (see Asplund et al. 2009). The choice is in agreement with [Fe/H] = −1.50 given by Sneden et al. (2004) and Harris (1996, as updated in 2010) for M 3.

We first fit the MS in order to fix the reddening, E(B-V), distance modulus, (m−$M_V$), and age. With our choice of isochrones we obtain: E(B-V)=0.008, (m − $M_V$) = 15.07 and Age = 11.0 Gyr (Figure 2).

We compare the data of the HB stars and RRL variables with a large array of simulations, arranged on a grid, where the parameters we can not constrain directly from the observations are progressively changed. In detail, the grids are built by varying the mass loss in steps of 0.001 $M_{\odot}$: we changed the mass loss of the 1G stars from $\mu_{1G}$ = 0.160 to 0.220 $M_{\odot}$ and the mass loss of the 2G samples from $\mu_{2G}$ = 0.180 to 0.260 $M_{\odot}$. The mass loss spread for the 1G ($\sigma^{\mu}_{1G}$) and/or for the 2G samples ($\sigma^{\mu}_{2G}$) is changed in steps of 0.001 $M_{\odot}$ from 0.000 to 0.010 $M_{\odot}$. This allows to constrain quantitatively the difference in mass loss between the different groups. We assess the quality of each simulation in the grid both comparing the histograms in the figures and performing a series of KS tests.

|        | HBR   | $\bar{M}_{HB}^{1G}/M_\odot$ | $\bar{M}_{HB}^{2G}/M_\odot$ | $\delta\bar{Y}_{1G}$ | $\delta\bar{Y}_{2G}$ | $\bar{P}_{RRL}$/days | $\bar{M}_V^{RRL}$ | $p_{KS1}$  | $p_{KS2}$ | $p_{KS3}$ |
|--------|-------|--------|--------|-----------|--------|--------|-------|-----------|-------|---------|
| Sim.1  | 0.322 | 0.659  | 0.621  | ~ 0.000   | 0.016  | 0.532  | 15.66 | 0.87      | 0.84  | 0.92    |
| Sim.2  | 0.649 | 0.624  | 0.621  | 0.026     | 0.016  | 0.507  | 15.63 | << 0.001  | 0.09  | 0.03    |
| Sim.2.2| 0.462 | 0.651  | 0.621  | 0.018     | 0.016  | 0.505  | 15.64 | 0.05      | 0.02  | < 0.001 |
| Sim.3  | 0.517 | 0.636  | 0.621  | 0.026     | 0.016  | 0.521  | 15.61 | 0.02      | 0.04  | < 0.001 |
| Sim.4  | 0.506 | 0.641  | 0.621  | 0.013     | 0.016  | 0.525  | 15.67 | 0.007     | 0.56  | 0.77    |
| Sim.5  | 0.384 | 0.651  | 0.621  | 0.013     | 0.016  | 0.532  | 15.66 | 0.60      | 0.58  | 0.95    |

**Table 2.** Some general parameters of the simulations shown in § 3 and 4. Columns are: the value of HBR, the mean value of mass ($M_{HB}$) and helium enrichment ($\delta Y$) for both the 1G and the 2G stars, the mean value of the RRL period ($P_{RRL}$), the mean V magnitude of the RRL variable and the p values from the three KS test we perform during our analysis.

Once we have analysed the HB data of this cluster, we will test if our findings are adequate to describe the MS as well. To do so, we perform a series of MS simulations following the recipes described in Tailo et al. (2016). The procedure requires only the assumption of an exponent for the mass function ($\zeta$). In this case we adopt $\zeta = -0.7$, the same exponent Tailo et al. (2016) used for $\omega$ Centauri. Photometric errors have been evaluated with the artificial star procedure developed in Anderson et al. (2008). We also introduce in the simulation the binary fraction found for M3 by Milone et al. (2012, ~ 3.5%).

# 3   RESULTS: SIMULATIONS WITH NO HELIUM SPREAD IN THE 1G

We start examining the case where the 1G has a very small or no helium spread. The observational constraints are summarized as follows:

• The mean and the max value of $\Delta Y$ between the 1G and the 2G stars as obtained by Milone et al. (2018, Table 4): $\Delta Y_{2G,1G} = 0.016 \pm 0.005$ and $\Delta Y_{2G,1G}^{max} = 0.041 \pm 0.009$ .
• The colour distribution of HB stars in M3, as seen in Fig. 1b.
• The value of HBR as calculated from the *HST* sample: $0.313 \pm 0.034$.
• The period distribution of our sample of RRL as extracted from Benkő et al. (2006) and reported in Fig.1c.
• The V magnitude distribution the RRL as extracted from Benkő et al. (2006) (see Fig. 1d).

We first examine several simulations containing only 1G stars to locate them on the HB. Given that both their helium mass fraction (Y ~ 0.25) and its spread ($\sigma^Y$ ~ 0.00) can be constrained, the only remaining free parameters are the values of mass loss and its spread ($\mu_{1G}; \sigma_{1G}^\mu$), which are constrained with the help of the simulation grid described in § 2.2. We locate these stars on the red HB, and further constrain the values of these parameters with the RRL period and mean magnitude distributions.

We now repeat the process including the 2G stars. The simple two populations model we adopted for the M4 case (Tailo et al. 2019) does not work here as the morphology of the HB locus is more complex. We then need to split the blue HB stars in few groups ($2G_A$, $2G_B$, $2G_C$) with the 'A' group hosting the majority (~ 90%) of them. The helium abundances of these three groups are chosen in agreement to the $\Delta Y_{2G,1G}$ and $\Delta Y_{2G,1G}^{max}$ values mentioned before: we give

the highest value to the bluest group of stars ($2G_C$) and we assign to the $2G_A$ group a value close to $\Delta Y_{2G,1G}$ measured in Milone et al. (2018). Finally we give to the $2G_B$ group an intermediate value. The final helium mass fraction values are listed in Table 1.

Once the values of Y are set, the only free parameters remaining are the mass loss of the 2G stars and its spread ($\mu_{2G}; \sigma_{2G}^\mu$, for each group). We constrain these values by iteratively comparing the data with a new simulation grid which includes these new groups.

Our best fit simulation (Sim. 1) is the one where $\mu_{1G} = 0.188 \ M_\odot$. The mass loss of the 2GA, 2GB and 2GC groups is 0.016, 0.042 and 0.052 $M_\odot$ larger, respectively. The other inputs used are reported in (see Table 1). This confirms our previous findings in Tailo et al. (2019).

We apply the same procedure we used in Tailo et al. (2019) to evaluate the errors on these estimates and we obtain $\delta\mu_{1G,2GA} = 0.016 \pm 0.007 M_\odot$, $\delta\mu_{1G,2GB} = 0.032 \pm 0.009 M_\odot$ and $\delta\mu_{1G,2GC} = 0.052 \pm 0.013 M_\odot$ The results of Sim. 1 are represented in Figure 3; we also report some general parameters of this simulation in Table 2.

Figure 3a describes the simulated HB in the F336W and F814W CMD. The filled black dots indicate the observations while the open black dots indicate the variables. The simulation points are colour coded to distinguish the 1G and the 2G stars (red squares and the green triangles, respectively). The simulated RRL variables are represented by the open squares and triangles. The blue histogram is the colour distribution of the simulated, non variable, HB stars. The comparison with the homologous distribution for the data, the black shaded histogram, shows a good agreement, confirmed by the high probability value obtained from the KS test ($p_{KS1}$, see Table 2) for the two series of points. Furthermore, we obtain HBR = 0.322, in agreement with the observed value. Note that the mass distribution of the 1G and 2G stars is different. The 1G stars have, on average, higher masses than the 2G ones (see Table 2). In addition the value of $\delta\bar{Y}_{2G}$ is in agreement with the value given in § 2.1.

Sim.1 contains ~ 100 RRL variables, a number compatible with the observed sample. Fig. 3b shows that the observed and simulated period distribution are in good agreement, also testified by the high probability value we obtain from the KS test ($p_{KS2}$) and the similar mean period value (see Table 2). A good agreement is also found for the mean magnitude distribution of the variables (Fig. 3c), again confirmed by the high value of the KS test p-value ($p_{KS3}$).

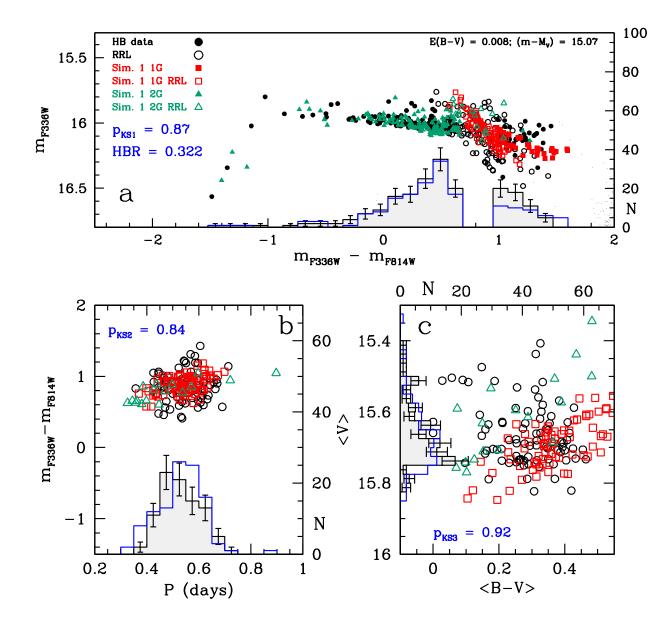In summary, we have shown that a standard descrip-

**Figure 3.** *Panel a:* The results of Sim.1. In the panel, the data are represented as black circles (solid for the HB stars and open for the variables) while the 1G and the 2G stars present in the simulation are the red square and the green triangles, respectively. We represent the variables of the simulation with open points as well. The two histograms, shaded black and blue, respectively for the data and the simulation, describe the agreement between the two sets of points. We reach a satisfying reproduction of the HB morphology. The final inputs used are listed in Table 1. *Panel b:* The RRL variables in the *HST* sample and in Sim.1 observed in the P vs ($m_{F336W} - m_{F438W}$) plane. The histograms in the panel describe their period distribution. *Panel c:* The CMD obtained from the average B and V magnitude of the simulated and the observed RRL variables. The histograms in the panel describe the V magnitude distribution of both samples.

tion of the HB in M 3, assuming a single–valued helium content for 1G stars, and a helium enhancement consistent with the observational results describes in a satisfactory way the colour distribution and the RRL variables, as found in previous work on this cluster (e.g. Catelan 2004; Castellani et al. 2005; Caloi & D'Antona 2008; Denissenkov et al. 2017), although adopting slightly different input parameters (see § 6).

## 4  INTRODUCING THE HELIUM SPREAD IN 1G STARS

We now add a new constraint to the simulations: an internal helium spread among 1G stars. The spread has been computed by using the ChM map of 1G stars, by assuming that their distribution along the ($m_{F275W} - m_{F814W}$) colour (see Fig. 1a) is due to helium variation.

We assign a standard helium value to those stars with $\Delta_{F275W,F814W} > -0.03$. This choice is made following the in-
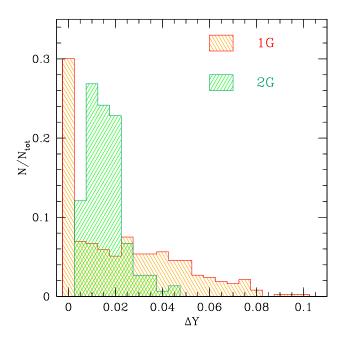
**Figure 4.** The distribution of helium enhancement ($\Delta Y$) of the 1G (red) and 2G stars (green) calculated in this work. See text for further details.

dication from the error distribution in Figure 8 in Milone et al. (2018, and references therein). We then assign the maximum value measured in Milone et al. (2018), $\sim 0.1$, to the bluest star in the 1G sample, located at $\Delta_{F275W,F814W} \sim -0.4$. We linearly interpolate the helium value for the stars with $-0.4 < \Delta_{F275W,F814W} < -0.03$. The distribution is shown in Figure 4, where it is compared with the analogous distribution for the 2G stars; $\sim 30\%$ of the 1G stars preserve a standard helium content. We now attempt to achieve a new fit of the HB by including this 1G helium spread. The inputs of the simulations from 2 to 5 are reported in Table 1 and some of their general properties in Table 2.

### 4.1 Sim. 2: including the 1G helium spread into Sim. 1

Figure 5 shows what happens by simply including the 1G helium spread, but leaving unaltered the other inputs of Sim. 1. Now HBR $\sim 0.649$, significantly higher than the observed value because a good fraction of the of red HB stars goes to overpopulate the blue region; also the KS test confirms a very low probability value. In fact, the stars with larger helium have smaller masses and occupy bluer positions along the HB, as we have left the mass loss of all the 1G stars unaltered (see Table 2).

Sim. 2 has $\sim 70$ RRL variables, a number too small to be compatible with the observed sample. The period distribution is described in Fig. 5b. The histograms in the panel testify that the simulated distribution is not a good description of the observed one for it is too wide. The discrepancy between the simulated and the observed variable stars is also indicated by the different distribution of their mean magnitudes (see Table 2). Fig. 5c describes, as in the previous case, the distribution in $M_V$ for the two samples. We see that the

simulated ones do not have the peak we observe; the discrepancy is also confirmed by the low KS probability value (see Table 2).

To further explore how Sim. 1 changes, we realize a simulation using a distribution with a lower maximum, i.e. the one suggested by the findings in Lardo et al. (2018). We obtain a simulated HB with $\sim 100$ RRL and HBR $\sim 0.46$; the latter is too high to be considered in agreement with the observed value. Furthermore, the low probability values we obtain from the KS tests for this new simulation (Sim. 2.2 in Table 2) indicate a strong discrepancy with the observations also in this case.

### 4.2 Sim. 3: lowering the 1G mass loss

Since one of the main issues of Sim. 2 is the low number of red HB stars, we test if a simulation with a lower mass loss value, for now arbitrarily chosen, would work. Sim. 3 adopts $\mu_{1G} = 0.175 M_\odot$ and the other inputs listed in Table 1. The rHB stars are better reproduced, but we are still overpopulating the blue HB, obtaining a HBR $= 0.517$. The number of RRL variables is even smaller than in Sim.2, $\sim 45$, thus Sim. 3 is not a good description of the observations, and in fact the KS tests report low probability values(see Table 2). If we lower the $\mu_{1G}$ even more, the HBR value would be lowered as well, but the number of RRL variables would become lower too, thus representing a worse description. In the same manner an higher value of $\mu_{1G}$ would produce even higher values of HBR, producing a worse simulation as well. We therefore have to reject this simulation, and try a different approach.

### 4.3 Sim. 4: starting the simulation from the variable stars distribution

Because the majority ($\sim 80\%$) of the RRL variable occupies the lower luminosity part of the strip (Fig. 1d), we can assign them ($\sim 75$) to the standard helium part of the 1G. We then give to the remaining stars in the 1G of Sim.1 ($\sim 55$) the helium spread previously derived (Figure 4). We leave the 2G inputs untouched: this gives us an additional $\sim 15$ RRL variables for a total of $\sim 90$ RRL, a number compatible with the observed sample.

By using the same procedure adopted for Sim.1, we obtained the values of $\mu_{1G}^{RRL}$ and $\sigma_{1G}^{\mu^{RRL}}$ necessary to reproduce the features of the observed RRL variables. We then use these values to simulate the rest of the 1G stars. We obtain a good fit of the variables with $\mu_{1G}^{RRL} = 0.189 M_\odot$. This result is unsurprisingly similar to the value we obtain in Sim.1; due to the fact that the RRL features are among our main constraints. The other inputs used in this simulation (Sim. 4) are listed in Table 1 and the results reported in Figure 6, which follows the format of the previous ones.

Figure 6b and 6c confirm that the features of the RRL variable in Sim.4 are in a good agreement with the observations (by construction), as confirmed by the high probability values of the KS tests reported Table 2. Unfortunately, as shown in Figure 6a, with these values of $\mu_{1G}^{RRL}$ and $\sigma_{1G}^{\mu^{RRL}}$, the number of red HB stars is smaller than the observed one, while the blue HB is overpopulated (HBR = 0.506, still
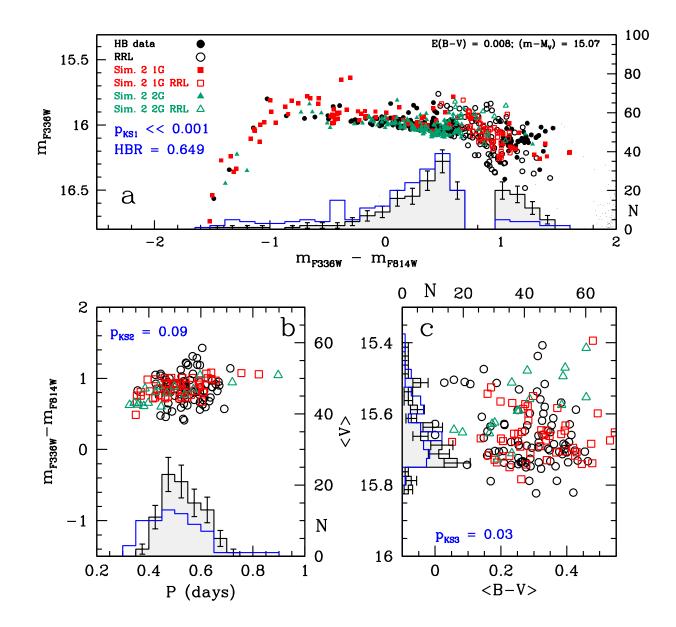
**Figure 5.** As Figure 3 but for Sim. 2.

significantly higher than observed). The corresponding KS probability is $p_{KS1} \sim 0.007$, see Table 2.

### 4.4  Sim. 5: lowering the mass loss of the red HB, with respect to Sim. 4

We attempt to improve the fit by lowering the mass loss of the non variable (NV) 1G stars. We repeat the procedure of Sim.1 including this new group of stars and find a good fit with $\mu_{1G}^{NV} = 0.171\,M_{\odot}$. The other inputs of this new simulation (Sim.5) are reported in Table 1. Figure 7 reports its results.

As in the case of Sim. 4 we have that the RRL properties are well reproduced by construction (see Fig. 7b, Fig.

7c and Table 2). In Fig. 7a we report the simulated HB stars of Sim.5. Apparently, we have a good reproduction of the observed sample: we indeed obtain a high probability value from the KS test (see Table 2). We have HBR = 0.384, a value slightly higher than the observed one. Additional considerations, however, suggest that this simulation is not acceptable when framed in the context of GC evolution and the spectroscopic observations of M3. Indeed, for the non variable 1G stars, we reduced $\mu$ of a non negligible quantity ($\Delta\mu \sim -0.018\,M_{\odot}$). The current scenarios for the 1G formation describe those stars formed in the same environment. It is then unlikely that stars in the same generation suffer such diverse mass loss.

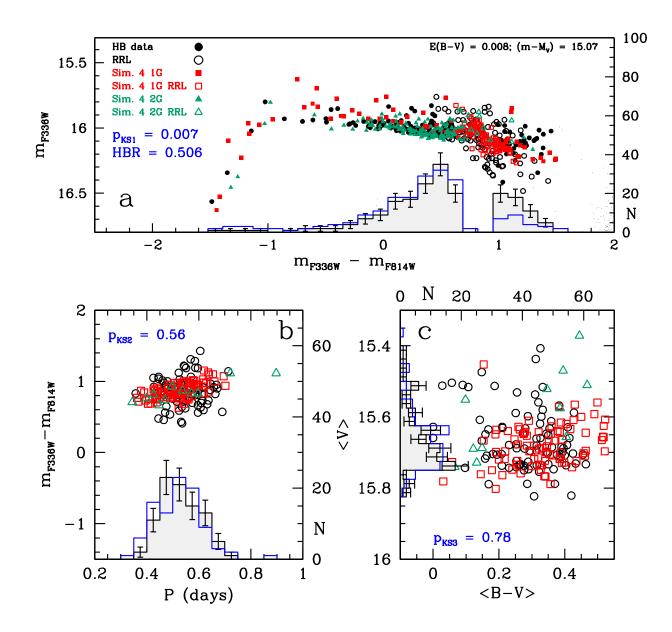The need to reduce the mass loss can be avoided if we

**Figure 6.** As Figure 3 but for Sim. 4.

change the value of $M_{Tip}$ between the RRL and the non variable stars. This can be achieved in two ways: assuming they are *younger* or *increasing their metallicity*. From our isochrones database we found that an age difference of $\sim -1.0$ Gyr would produce the same effects; similarly with $\delta$[Fe/H] $\sim 0.18$. Both these possibilities have to be excluded because, at the time of this writing, they are not supported by the current spectroscopic and photometric observational framework for M3.

Furthermore, there is no evidence that a significant variation of [C+N+O/Fe] has been directly observed within the 1G, see Marino et al. (2019) and Cabrera-Ziri et al. (2019), for the case of NGC 2808). Thus as aforementioned, we then need to reject this simulation as unsatisfactory.

## 5 THE MS COUNTERPARTS OF THE HB SIMULATIONS

Now that we have a description of the stellar populations hosted in the HB of M 3, we check if our findings are adequate to describe the MS as well. We analyse the MS counterpart of Sim.1 and Sim.2 and compare them to the MS data in the F606W and F814W bands. We will perform the simulations as previously described (see § 2.2), dividing the total number of MS stars in the groups listed in Table 1.

Figures 8 and 9 report the results of these new tests. The left panel of both figures reports the MS data of M 3; the central panel describes these new simulations, $Sim_{MS}1$ and $Sim_{MS}2$, respectively for Fig. 8 and 9. In the panels, the yellow line represents the fiducial of the data. The red, blue
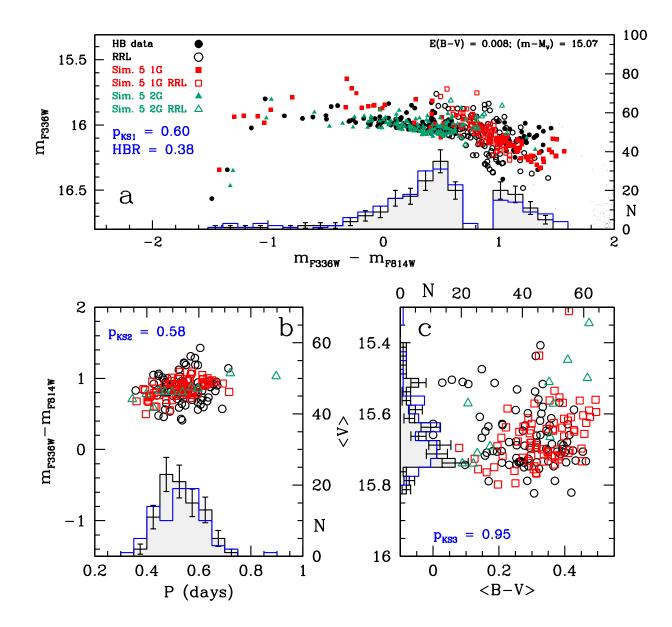
**Figure 7.** As Figure 3 but for Sim. 5.

and black lines are the isochrones with Y=0.25, 0.28 and 0.35, respectively. As in previous figures, the 1G and the 2G are represented as red and green dots, respectively. The histograms on the right panels compare the $\Delta_{m_{F606W}-m_{F814W}}$ distribution of both the data, grey, and the simulations, blue.

We immediately see that in $Sim_{MS}2$ the 1G overlaps with the 2G entirely, populating even the blue side of the MS. This is the direct consequence of its helium distribution. Indeed, in $Sim_{MS}2$, the 1G stars have, on average, higher helium mass fraction values than the ones in $Sim_{MS}1$ and their counterparts in the 2G (see Tab. 2). The net result is that the blue side of the simulated MS is overpopulated compared to the observed one, as the comparison of the histograms in the figures shows. This simple test reinforces

the point we made with the HB simulations in the previous sections.

## 6 DISCUSSION AND CONCLUSIONS

We present a collection of HB and MS simulations to investigate whether the tentative interpretation of the 1G colour extension observed in the ChM of M 3 in terms of a pure helium spread (Milone et al. 2015; Lardo et al. 2018; Milone et al. 2018) is consistent with other observations of this clus-
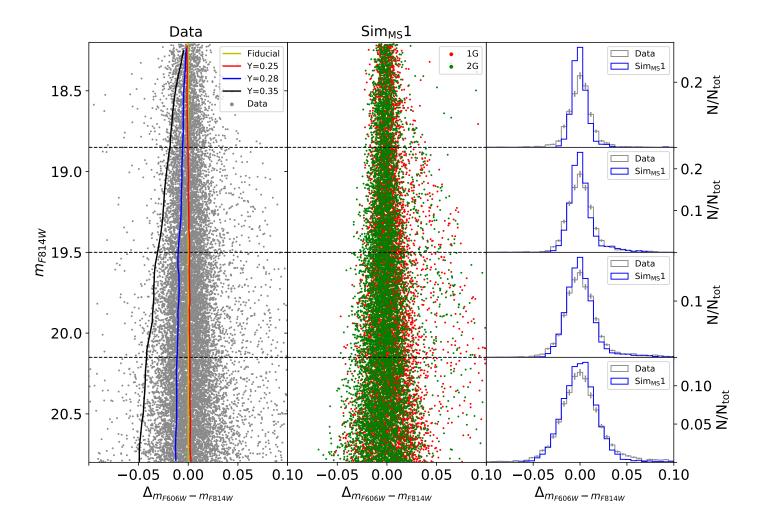
**Figure 8.** *Left and central panels:* The comparison of the MS counterparts of Sim.1, dubbed Sim$_{MS}$1, with the MS data of M 3. The yellow line in the panel represents the fiducial of the data, while the red, blue and black ones are the isochrones with Y=0.25,0.28 and 0.35 respectively. *Right panel:* The histograms compare the $\Delta_{m_{F606W}-m_{F814W}}$ distribution of the data, grey, and Sim$_{MS}$1, blue in the four intervals of magnitudes highlighted in the panel.

ter. The parameters of our simulations must be chosen in order to satisfy the following observational constraints[3]:

• the mean and the max value of **ΔY** between the 1G and the 2G stars as obtained by Milone et al. (2018, Table 4);
• the colour distribution of the HB stars in M3 and the value of the HB ratio of our sample;
• the period and mean magnitude distributions of our RRL sample.

The parameters which can not be directly constrained from these observations, namely the mass loss of the 1G and the 2G star groups with their dispersion ($\mu_{1G(2G)}$ and $\sigma^{\mu}_{1G(2G)}$), have been constrained by iteratively comparing a series of simulation grids with the data. We have thus shown only the

most representative results of a large and deep exploration of the parameters space.

The main result of this work is that there is no combination of parameters that reproduces correctly all the observational constraints at the same time, *if we include within the 1G stars the internal helium spread suggested by the most direct interpretation of the Chromosome Map.* We conclude that the reasons for the colour spread of the 1G remain to be understood. We, instead, find that any helium spread associated with the 1G stars in Sim. 1 has to be very small (<0.002). This also rules out the possibility that a smaller but non negligible helium enhancement (as the one described by Lardo et al. 2018) can be used to describe the 1G stars in this cluster.

The simulations we show in this work have other interesting features:

(i) When the 1G stars have small or no helium spread, all
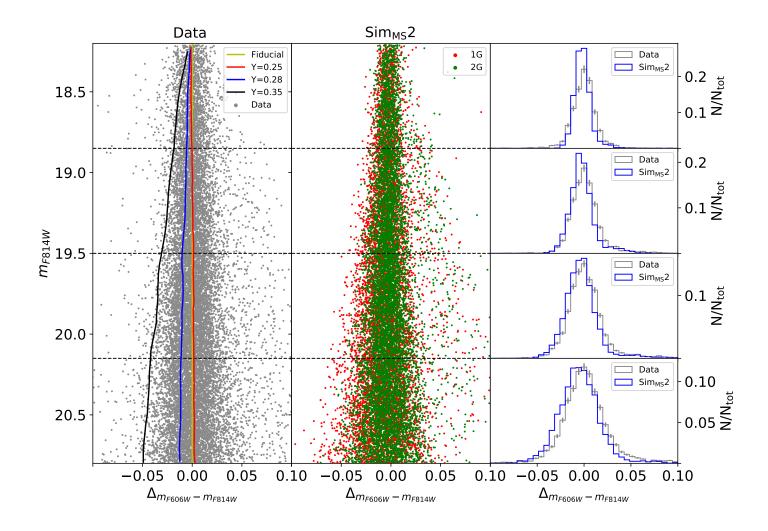
---

[3] described in §2.1

**Figure 9.** As Fig. 8 but for the MS counterpart of Sim. 2 (Sim$_{MS}$2)

the red HB stars and the majority of RRL variables belong to 1G. This result also confirms the approach already followed by different authors in the past (e.g. Caloi & D'Antona 2008; Denissenkov et al. 2017). The mass loss needed to reproduce the position on the HB of the 1G star locates them near the red border of the instability strip.

(ii) We find that the mass loss spread for the two population has to be small ($\sigma^\mu \sim 0.005 M_\odot$). This value is larger than the one from Caloi & D'Antona (2008) ($\sigma^\mu \lesssim 0.003 M_\odot$), thanks to the lower peak of the period distribution of RRL variables. On the other hand, VandenBerg et al. (2016) and Denissenkov et al. (2017) found a larger value ($\sigma^\mu \sim 0.008 M_\odot$ in their 1G). This is consequence of adopting the catalogue from Cacciari et al. (2005), who are interested in the accurate photometry of these stars and thus exclude the variables which show the Blazhko type variability (Blažko 1907) from the number versus period distribution of RRL. Although the colours of these stars are more difficult to be measured with accuracy, the periods of these RRL variables are well known and contained in the complete

Benkő et al. (2006) catalogue. Discarding the Blazhko RRL ($\sim 30\%$ of the sample), the number versus period distribution becomes flatter, and is consistent with a larger value of $\sigma_\mu$.

(iii) Having both $\Delta Y_{2G,1G}$ and $\Delta Y_{2G,1G}^{max}$ fixed by the observations reported in Milone et al. (2018) we can also constrain the mass loss difference between the two populations. In Sim. 1 we find $\delta\mu_{1G,2GA} = 0.016 \pm 0.007 M_\odot$ and $\delta\mu_{1G,2GC} = 0.052 \pm 0.013 M_\odot$. The errors have been estimated with the procedure used in Tailo et al. (2019). All the other simulations show similar differences. We found a similar trend in the HB of the cluster M 4 (Tailo et al. 2019), hinting that this can be a common behaviour in GCs. Denissenkov et al. (2017) also found larger mass loss for the 2G stars in M 3. This difference in the mass loss is also consistent with the very small —if any— helium increase across the RRL variables region, found by Catelan et al. (2009), but does not rule out helium as a primary parameter to determine the morphology of the whole HB.

(iv) We regard the difference in mass loss between 1G

and 2G as a result of the different formation conditions of the two populations (e.g. different initial rotation rates, as we suggested in Tailo et al. 2015, 2016, 2017, 2019) . Consequently, we attribute the same mass loss to all 1G stars, even for the simulations with 1G helium spread. However, increasing values of mass loss for the helium rich stars in the 1G lead to even worse agreement with the observations, as the blue HB would include even more stars (thus obtaining an even higher HBR).

(v) The RRL variables in our simulations are made up almost entirely by 1G stars. In Sim.1 only 14 RRL ($\sim 15\%$) belong to the 2G. The 2G RRL are evolved HB stars, crossing the instability strip from the blue side and they are, on average, more luminous than their 1G counterparts.

(vi) Sim. 5 shows an almost adequate reproduction of the observed HB stars in M3, except for the value of HBR, which is slightly higher (0.384, see Fig. 7 and Table 2). To obtain this result, we needed to lower the mass loss of the non variable stars of a non negligible quantity ($\Delta\mu \sim -0.018$ M$_\odot$). At the time of this writing we can not justify this assumption within the current spectroscopic and photometric observational framework of M 3 therefore we have to reject this last simulation.

(vii) The simulations of the MS in Fig. 8 and 9, counterparts of Sim.1 and Sim.2, show that the blue MS would be overpopulated if the 1G includes a large helium spread, reinforcing the results obtained from the HB simulations.

In conclusion, the exam of the CMD data of M 3, in particular its HB stellar distribution, the period distribution of its RR Lyrae variable stars, and the color distribution of the main sequence stars, do not support the hypothesis that the color spread of the 1G is due to internal helium variations among this population, thus the problem remains to be understood.

Notice that M 3 and M 13 are the most typical example of "second parameter" pair (e.g. see the now classic work from Caloi & D'Antona 2005), and, while M 3 has an extended 1G, M 13 has a very compact 1G (see the reproduction of their ChM in Milone et al. 2017, 2018). Is the 1G extension part of the (still unsolved) "second parameter" problem?

## ACKNOWLEDGEMENTS

## REFERENCES

Anderson J., et al., 2008, AJ, 135, 2055
Asplund M., Grevesse N., Sauval A. J., Scott P., 2009, ARA&A, 47, 481
Benkő J. M., Bakos G. Á., Nuspl J., 2006, MNRAS, 372, 1657

Blažko S., 1907, Astronomische Nachrichten, 175, 325
Buonanno R., Corsi C. E., Buzzoni A., Cacciari C., Ferraro F. R., Fusi Pecci F., 1994, A&A, 290, 69
Cabrera-Ziri I., Lardo C., Mucciarelli A., 2019, MNRAS, 485, 4128
Cacciari C., Corwin T. M., Carney B. W., 2005, AJ, 129, 267
Caloi V., D'Antona F., 2005, A&A, 435, 987
Caloi V., D'Antona F., 2008, ApJ, 673, 847
Castellani M., Castellani V., Cassisi S., 2005, A&A, 437, 1017
Catelan M., 2004, ApJ, 600, 409
Catelan M., Ferraro F. R., Rood R. T., 2001, ApJ, 560, 970
Catelan M., Grundahl F., Sweigart A. V., Valcarce A. A. R., Cortés C., 2009, ApJ, 695, L97
Corwin T. M., Carney B. W., 2001, AJ, 122, 3183
D'Antona F., Caloi V., Montalbán J., Ventura P., Gratton R., 2002, A&A, 395, 69
D'Antona F., Bellazzini M., Caloi V., Pecci F. F., Galleti S., Rood R. T., 2005, ApJ, 631, 868
D'Antona F., Vesperini E., D'Ercole A., Ventura P., Milone A. P., Marino A. F., Tailo M., 2016, MNRAS, 458, 2122
D'Ercole A., Vesperini E., D'Antona F., McMillan S. L. W., Recchi S., 2008, MNRAS, 391, 825
Denissenkov P. A., VandenBerg D. A., Kopacki G., Ferguson J. W., 2017, ApJ, 849, 159
Ferraro F. R., et al., 1997, A&A, 324, 915
Harris W. E., 1996, AJ, 112, 1487
Lardo C., Salaris M., Bastian N., Mucciarelli A., Dalessandro E., Cabrera-Ziri I., 2018, A&A, 616, A168
Lee J.-W., 2019, ApJ, 872, 41
Marconi M., et al., 2015, ApJ, 808, 50
Marino A. F., et al., 2019, arXiv e-prints,
Mazzitelli I., D'Antona F., Ventura P., 1999, A&A, 348, 846
Milone A. P., et al., 2012, A&A, 540, A16
Milone A. P., et al., 2015, ApJ, 808, 51
Milone A. P., et al., 2017, MNRAS, 464, 3636
Milone A. P., et al., 2018, MNRAS,
Piotto G., et al., 2015, AJ, 149, 91
Sneden C., Kraft R. P., Guhathakurta P., Peterson R. C., Fulbright J. P., 2004, AJ, 127, 2162
Tailo M., et al., 2015, Nature, 523, 318
Tailo M., Di Criscienzo M., D'Antona F., Caloi V., Ventura P., 2016, MNRAS, 457, 4525
Tailo M., et al., 2017, MNRAS, 465, 1046
Tailo M., Milone A. P., Marino A. F., D'Antona F., Lagioia E., Cordoni G., 2019, arXiv e-prints,
VandenBerg D. A., Denissenkov P. A., Catelan M., 2016, ApJ, 827, 2
Ventura P., Zeppieri A., Mazzitelli I., D'Antona F., 1998, A&A, 334, 953
Vesperini E., McMillan S. L. W., D'Antona F., D'Ercole A., 2013, MNRAS, 429, 1913

This paper has been typeset from a TeX/LaTeX file prepared by the author.